Texila International Journal | Open Access | Peer Reviewed

Journal: Texila International Journal of Academic Research
https://doi.org/10.21522/TIJAR.2014.13.03.Art007

ISSN: 2520-3088
Volume 13 Issue 3, 2026

A Comparative Study of Synthesized Berberine-Iron Oxide Nanoparticles and Cisplatin: Characterization and Biological Applications

Malchi Suresh[1], Manju Bargavi Sakthivel[2], Tippavarjula HemaHarshitha[3], Gauravaram Avinash[4], Devarajan Nalini[1*]

[1]*Department of Research, Meenakshi Academy of Higher Education and Research, K. K. Nagar, Chennai, Tamil Nadu 600078, India*

[2]*Department of Nutrition and Dietetics, Meenakshi Academy of Higher Education and Research, K. K. Nagar, Chennai, Tamil Nadu 600078, India*

[3]*Department of Biochemistry, Government Medical College, Suryapet, Thallagadda, Telangana-508213, India*

[4]*Department of Microbiology, Narayana Medical College, Nellore, Andhra Pradesh 524305, India*

***Correspondence to be addressed:** E-mail - drnalini.crl@madch.edu.in

Cite this article as: Malchi S, Sakthivel MB, HemaHarshitha T, Avinash G, Nalini D. A comparative study of synthesized berberine-iron oxide nanoparticles and cisplatin: characterization and biological applications. Texila Int J Acad Res. 2026;13(3). https://doi.org/10.21522/TIJAR.2014.13.03.Art007

Received: 28.02.2026
Accepted: 09.03.2026
Published: 31.07.2026

Abstract *Non-small cell lung cancer (NSCLC) remains one of the leading causes of cancer-related deaths worldwide due to its high incidence, aggressive progression, and limited treatment options. Although cisplatin-based chemotherapy is a standard treatment for NSCLC, its clinical use is hindered by severe side effects and drug resistance. To address these challenges, the present study focused on the green synthesis of berberine-loaded iron oxide nanoparticles (BBR-FeONPs) using Phyllanthus amarus as a natural reducing and stabilizing agent. The formation of BBR-FeONPs was indicated by a visible color change and confirmed through characterization techniques, including UV-visible spectroscopy, FTIR, XRD, SEM, TEM, and zeta potential analysis. UV-vis spectroscopy showed a surface plasmon resonance peak at 335-342 nm, while FTIR identified functional groups involved in nanoparticle stabilization. XRD confirmed their crystalline structure, and SEM/TEM analyses revealed spherical and oval-shaped particles with an average size of 52 ± 2 nm. Zeta potential analysis (-8.50 mV) indicated moderate colloidal stability. Antimicrobial assays showed dose-dependent inhibition zones against S. aureus (13.0 mm), E. coli (14.3 mm), and P. aeruginosa (15.0 mm). In vitro cytotoxicity studies demonstrated enhanced anticancer activity of BBR-FeONPs against H460 NSCLC cells (IC_{50}=34.27 ± 2 µg/mL) compared to BBR, FeONPs, and cisplatin, with lower toxicity toward HEK-293 normal cells. Wound healing assays showed significant anti-migratory activity (6.14% at 200 µg/mL). These findings suggest that BBR-FeONPs are a promising and safer alternative for NSCLC treatment. Further studies are needed to explore their molecular mechanisms, assess in vivo toxicity, and evaluate biodistribution profiles.*

Keywords *BBR-FeONPs, Berberine, Cisplatin, FeONPs, Wound Healing*.

This article is published under Creative Commons Attribution License (CC BY 4.0)

https://doi.org/10.21522/TIJAR.2014.13.03.Art007

Introduction

Lung cancer is the most commonly occurring cancer around the world [1, 2]. According to the Indian Council of Medical Research's National Cancer Registry Programme, the incidence of cancer in India is expected to rise from approximately 1.46 million cases in 2022 to 1.57 million by 2025, indicating a rising trend in the national cancer burden [3]. In India, metropolitan cities reported high lung cancer prevalence; Mizoram has the highest reported increasing lung cancer rates for both men and women when compared to Chennai, Delhi, and Bengaluru [4]. The major risk factors for lung cancer include occupational exposure to carcinogens such as asbestos, silica, air pollution, and genetic mutations; additionally, a high intake of processed meats and alcohol has been linked to an increased risk of developing lung cancer [5, 6]**.** Currently, NSCLC treatment options include both surgical interventions and non-surgical therapies such as radiation therapy, chemotherapy, targeted therapy, and immunotherapy. However, these approaches have often shown limited effectiveness due to a major challenge in drug resistance [7].

In recent years, nanotechnology has played an important role in enhancing NSCLC treatment, particularly in overcoming drug resistance. Nanoparticles can carry cancer-related drugs directly to tumour cells, reducing side effects and increasing therapeutic efficacy. Additionally, they help to overcome resistance mechanisms by improving drug uptake and retention within cancer cells [8, 9]. Among the various methods, green synthesis has gained more significant attention due to its environmentally friendly, budget-friendly, and biocompatible nature. Plant-based nanoparticles show promising anticancer activity when compared to chemically synthesized nanoparticles [10].

Recently, studies have highlighted the green synthesis methods of metal and metal oxide nanoparticles, such as silver (AgNPs), gold (AuNPs), and iron oxide (FeONPs), demonstrating their potential for sustainable and eco-friendly applications in various biomedical and industrial fields [11]. A traditional Indian Medicinal plant, like *P. amarus*, belonging to the *Euphorbiaceae* family, contains various therapeutic and phytochemical properties, such as flavonoids, polyphenols, and alkaloids, which act as natural reducing and stabilizing agents in the synthesis of nanoparticles [11, 12]. Several studies have confirmed that biologically synthesized FeONPs exhibit anti-inflammatory, anti-cancer, and antioxidant properties against cancer cells by generating reactive oxygen species (ROS), impairing mitochondrial function, and activating apoptotic pathways. Furthermore, FeONPs enhance bioavailability and cellular uptake, offering a biocompatible and cost-effective platform for targeted cancer therapy. The synthesis of *P. amarus-mediated* FeONPs in cancer treatment supports sustainable nanotechnology for therapeutic nanocarriers with dual diagnostic and treatment in lung cancer [13].

Berberine is a widely used natural product of quinoline alkaloid compounds primarily derived from various plants of Berberis [14]. It contains several phytochemical components that contribute to its diverse pharmacological applications, including chemoprotective, hepatoprotective, antidiabetic, antibacterial, antioxidant, anti-inflammatory, and antiviral effects [15]. Researchers have recently explored plant-based compounds such as berberine, which has demonstrated strong anticancer activity by targeting multiple oncogenic pathways. However, their clinical application is hindered by low bioavailability and poor absorption. To overcome these limitations, nanotechnology-based drug delivery systems, such as iron oxide nanoparticles, offer a promising approach to enhance the therapeutic effectiveness of berberine [16].

Cisplatin is a chemotherapy drug widely used to treat various cancers such as lung,

ovarian, testicular, and head and neck cancers [17]. The main action of cisplatin in lung cancer is to bind to DNA to prevent replication, inducing the formation of ROS, activating DNA repair mechanisms, arresting the cell cycle, and stimulating apoptosis [18]. However, it has some limitations, including toxicity-related side effects and producing drug resistance, which can impact overall effectiveness on non-small cell lung cancer treatment [17].

In the present study, the main aim is to formulate green-synthesized BBR-FeONPs using an eco-friendly approach, and it was characterized and evaluated for their biological activity, such as anti-cancer and anti-migratory effects against non-small cell lung cancer (NSCLC-H460) and normal human embryonic kidney (HEK-293) cell lines compared with the standard chemotherapeutic drug cisplatin. Additionally, the antimicrobial activity of BBR-FeONPs was assessed against clinical pathogens, including *Escherichia coli*, *Staphylococcus aureus*, and *Pseudomonas aeruginosa*.

Materials and Methods

Green Synthesis of Iron Oxide Nanoparticles using Phyllanthus Amarus Extract

The *P. amarus* plant was obtained from the Tada local market in Andhra Pradesh, India, and authenticated (1026.10122401) at the Siddha Central Research Institute, Chennai. The plant was properly washed and cleaned with double-distilled water, cut into smaller pieces, air-dried, and powdered using a manual grinder. A 1000 mg powdered sample was boiled in 100 mL of double-distilled water at 60°C for 2 hours, and the solution was filtered through Whatman No. 1 filter paper and stored at 4°C for further use. Ferric chloride ($FeCl_3$-20 mmol) was dissolved in 50 mL of double-distilled water. The *P. amarus* extract was mixed with the $FeCl_3$ solution in a 1:1 ratio and incubated at 40°C for 48 hours, on an orbital shaker at 250 rpm, maintaining pH between 7.35 to 7.45.

Biosynthesis of Berberine-Loaded Iron Oxide Nanoparticles (BBR-FeONPs)

0.1 mg of berberine chloride (BBR-Cl) was dissolved in 1.5 mL of dimethyl sulfoxide (DMSO) and subsequently diluted with 3.5 mL of phosphate buffer saline (PBS) to obtain a 5 mL berberine chloride solution. The solution was vortexed for 15 minutes and then stirred on a magnetic stirrer for 1 hour. The prepared solution was mixed with FeONPs in a 1:1 ratio and subjected to sonication for 30 minutes. The final solution was oven-dried at 35°C for 5 hours, and the dried powdered sample was stored at room temperature.

Characterization of BBR-FeONPs

The synthesized berberine-loaded iron oxide nanoparticles (BBR-FeONPs) were characterized using analytical techniques. UV–Visible spectroscopy (Shimadzu UV-1900i, Japan) was performed in the 200–700 nm range to confirm nanoparticle formation. Functional groups were identified using Fourier Transform Infrared (FT-IR) spectroscopy (Josvok FTIR-1500, China) within the 4000–400 cm^1 range. X-ray diffraction (XRD, Bruker, Germany) with Cu-Kα radiation (2θ = 20–80°) was used to confirm the crystalline structure of the synthesized nanoparticles. The surface morphology was analysed using a scanning electron microscope (SEM, Carl Zeiss Sigma 300). High-resolution transmission electron microscopy (HR-TEM, Thermo Fisher F200S) was used to determine the size, shape, and structural features of the nanoparticles. The zeta potential was measured using a Zeta sizer (Malvern Instruments, ZS Explorer v4.0, UK) to evaluate the surface charge and stability of the nanoparticles.

Antibacterial Activity of BBR-FeONPs

The antibacterial efficacy of berberine-conjugated iron oxide nanoparticles (BBR-FeONPs) was evaluated using the agar well

diffusion method against *Escherichia coli*, *Streptococcus aureus*, and *Pseudomonas aeruginosa*. The bacterial strains were obtained from the Central Research Laboratory, Meenakshi Academy of Higher Education and Research (MAHER), Chennai, India. Fresh bacterial cultures were prepared in sterile peptone water and incubated at 37 °C for 18 hours in an orbital shaker incubator at 120–150 rpm. Mueller-Hinton Agar (MHA) plates were prepared, and wells of 6 mm diameter were created into the agar using a sterile 200 µL pipette tip. Each well was loaded with 200 µL of BBR-FeONPs at concentrations of (0, 50, 100, and 150 µg/mL). Amoxicillin was used as a positive control. The plates were incubated at 37 °C for 24 hours, after which the zone of inhibition (in mm) was measured using a digital antibiotic zone reader to determine antibacterial activity.

In Vitro Biocompatibility Analysis

Cell Culture

Non-small cell lung cancer cell lines (H460) and human embryonic kidney (HEK-293) cell lines were obtained from the National Centre for Cell Science (NCCS), Pune, India. Cell lines were grown in Dulbecco's Modified Eagle's Medium (DMEM) with heat-inactivated 10% (FBS) and 5% penicillin-streptomycin (10,000 U/mL) at 37°C under a 5% CO_2 supply in a humidified atmosphere until cell growth reached 80% confluence.

Cytotoxicity Assay

The cytotoxic effects of FeONPs, BBR, BBR-FeONPs, and cisplatin were evaluated in H460 non-small cell lung cancer (NSCLC) cells and HEK-293 human embryonic kidney cells using the MTT assay. Cells (7×10^3 cells/well) were seeded in a 96-well plate and incubated at 37°C in a humidified atmosphere containing 5% CO_2 for 24 hours to allow for cell attachment. Following incubation, cells were treated with different concentrations (0, 25, 50, 75, 100, 125, 150, 175, and 200 µg/mL) of the test compounds and incubated for an additional 24 hours. Untreated cells served as the control group. After treatment, the culture medium was discarded, and 100 µL of fresh medium was added to each well, followed by the addition of 10 µL of MTT reagent and the plate was incubated for 4hours at 37 °C. Subsequently, 100 µL of sodium dodecyl sulphate (SDS) solution was added to each well and the plates were further incubated for 4–18 hours at 37 °C. The absorbance was then measured at 570 nm using an ELISA microplate reader (iMARK Bio-reader, Model No. 21154). All experiments were conducted in triplicate. The percentage of cell inhibition was measured using the following formula: Cell Viability (%) = (OD of test sample) / (OD of control) × 100 [19].

Wound Healing Assay

The migratory capacity of H460 non-small cell lung cancer (NSCLC) cells was evaluated using a wound healing (scratch) assay. 5×10^6 cells were seeded into 6-well plates and incubated at 37 °C in a humidified atmosphere containing 5% CO_2 for 24 hours until the cells reached approximately 85–90% confluence. A sterile 200 µL micropipette tip was used to create a uniform scratch in the cell monolayer. Detached cells were gently removed by washing with phosphate-buffered saline (PBS). Subsequently, cells were treated with various concentrations of BBR-FeONPs (0.25, 50, 100, and 200 µg/mL). Cisplatin (200 µg/mL) served as a positive control. The plates were incubated at 37 °C, and wound closure was measured at 0, 24, and 48 hours using a phase-contrast microscope (Accu-Scope, EXI310F, USA). All experiments were performed in triplicate. The percentage of wound closure (relative cell migration) was calculated using image analysis software by comparing the wound area at each time point relative to the initial wound area.

Statistical Analysis

Analysis of data was carried out with SPSS Statistics v19. Continuous variables

https://doi.org/10.21522/TIJAR.2014.13.03.Art007

are presented as Mean ± SD. Normality of data was evaluated through the Shapiro-Wilk test. Parametric tests were utilized, with paired t-tests for intra-group analysis and one-way ANOVA for inter-group analysis. Significance was determined at $p < 0.05$. All experiments were performed in triplicates ($n = 3$).

Results

Biosynthesis and Physicochemical Characterization of BBR-FeONPs

The aqueous extract of *Phyllanthus amarus* was employed for the green synthesis of iron oxide nanoparticles (FeONPs), functioning as both a reducing and stabilizing agent. As shown in Figure 1. The visible colour transition from pale yellow to dark brown confirms the formation of FeONPs. The synthesized FeONPs were subsequently conjugated with berberine to produce berberine-loaded iron oxide nanoparticles (BBR-FeONPs) [20].

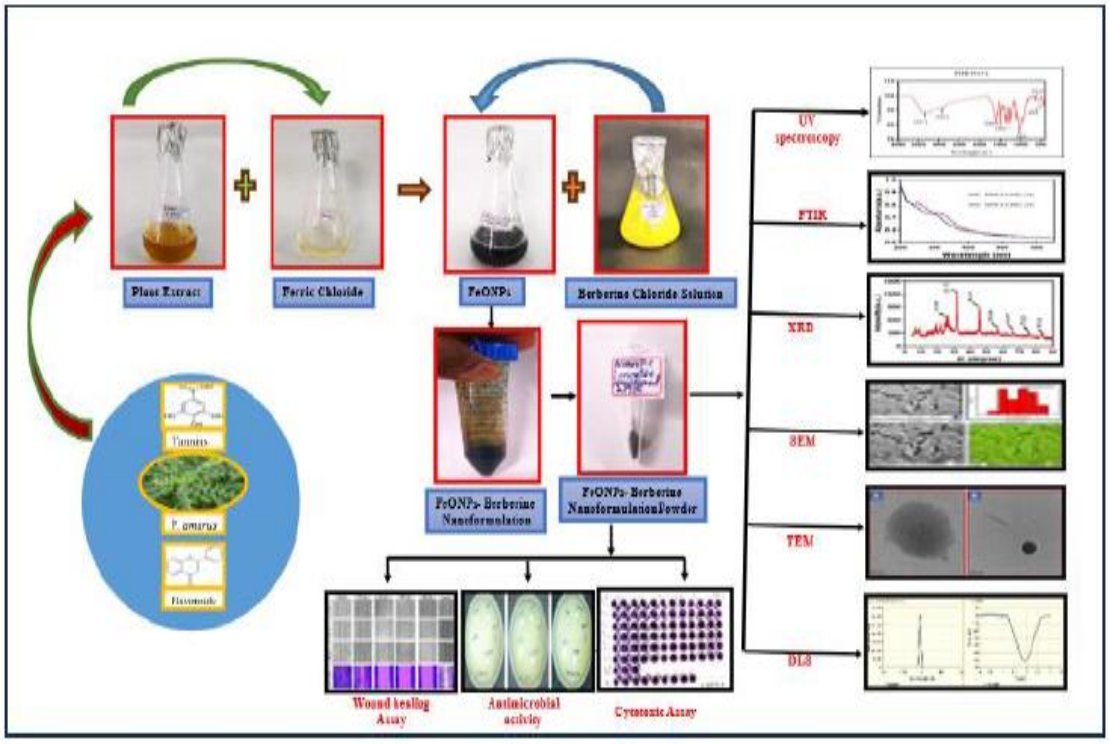

Figure 1. Synthesis of P. Amrus Mediated BBR-FeONPs

The characterization of BBR-FeONPs was investigated using UV-visible spectroscopy. The absorption spectra of FeONPs displayed a distinct peak around 275–285 nm, corresponding to the surface plasmon resonance (SPR) of iron oxide nanoparticles. The increased intensity and a slight redshift in the peak at 48 hours compared to 1 hour indicate progressive nanoparticle formation and stabilization. Upon conjugation with berberine, BBR-FeONPs exhibited characteristic absorption peaks at 335–342 nm, attributed to π–π^* electronic transitions of berberine. The observed redshift in the 6-hour sample compared to the 1-hour sample suggests successful interaction and conjugation of berberine with FeONPs, as shown in Figure 2 [21].

https://doi.org/10.21522/TIJAR.2014.13.03.Art007

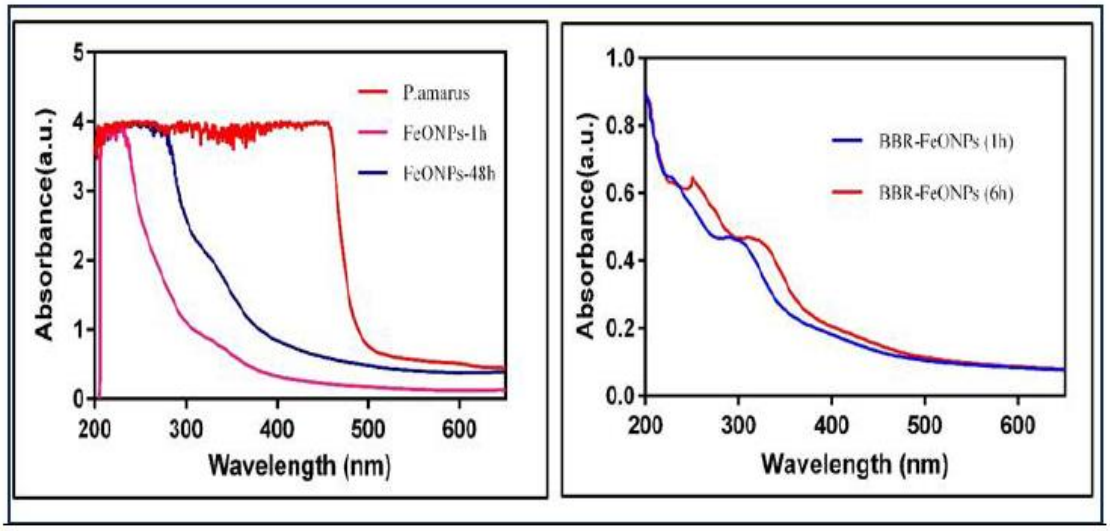

Figure 2. UV–Visible Spectroscopy of BBR-FeONPs

Fourier Transform Infrared (FTIR) spectroscopy was employed to confirm the functional groups involved in the FeONPs with berberine Figure 3. A broad absorption band at 3335.9 cm^{-1} corresponds to O–H stretching vibrations from hydroxyl groups, indicating the presence of phenolic or alcoholic compounds from berberine and *Phyllanthus amarus* extract. The peak at 2996.6 cm^{-1} is attributed to C–H stretching of aliphatic chains. Peaks at 1601.5 cm^{-1} and 1520.2 cm^{-1} correspond to C=C aromatic ring stretching, characteristic of the berberine structure. The bands at 1361 cm^{-1} and 1280.5 cm^{-1} are assigned to C–H bending vibrations of alkyl groups. A prominent band at 1040.2 cm^{-1} indicates C–O stretching, suggesting the involvement of alcohol, ether, or phenolic groups. The absorption peak at 621.3 cm^{-1} confirms the Fe–O stretching vibration, indicating the formation of iron oxide nanoparticles. These findings validate the successful capping and stabilization of FeONPs by berberine.

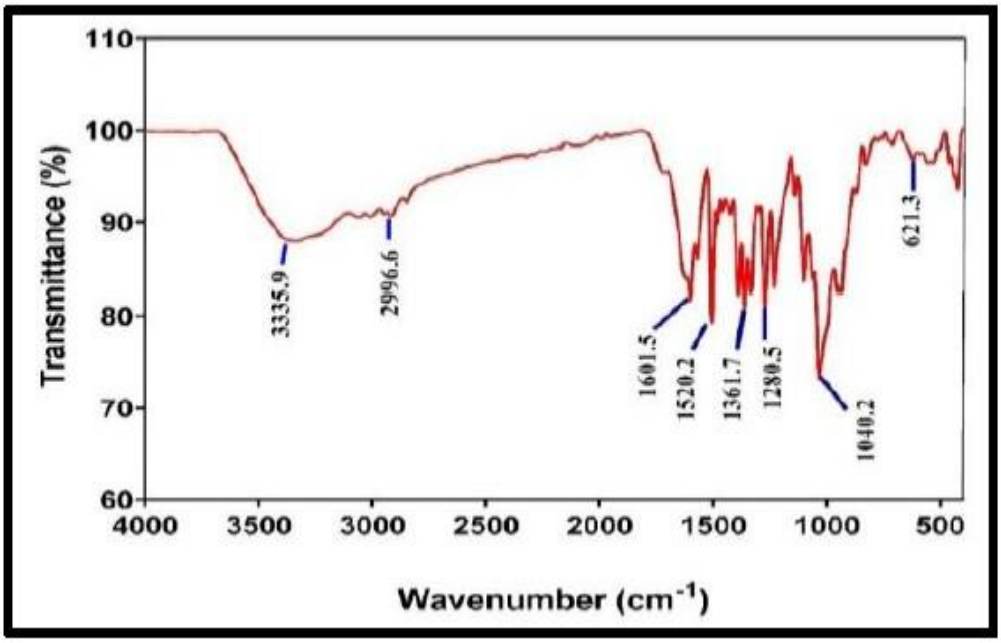

Figure 3. Fourier Transform Infrared Spectroscopy (FTIR) of BBR-FeONPs

https://doi.org/10.21522/TIJAR.2014.13.03.Art007

The crystalline structure of BBR-FeONPs was analysed using X-ray diffraction (XRD), as shown in Figure 4. The diffraction pattern exhibited distinct peaks at 2θ values of 29.48°, 33.72°, 46.41°, 58.44°, 66.89°, 76.23°, and 85.23°, corresponding to the crystallographic planes (100), (101), (102), (103), (110), (112), and (201), confirming the crystalline nature of the nanoparticles. The most intense peak at 33.72° (assigned to the (101) plane) was used to calculate the average crystallite size using the Debye–Scherrer equation, yielding an approximate size of 16.51 nm.

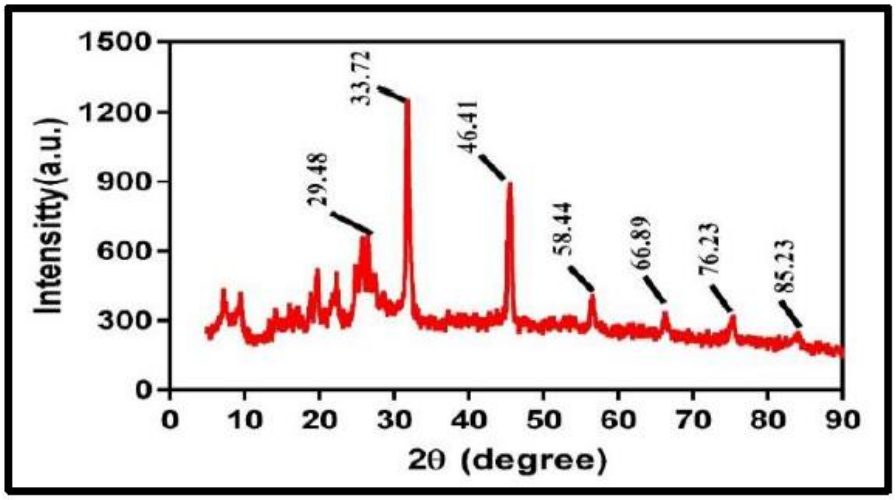

Figure 4. Energy Dispersive X-ray Spectrometry of BBR-FeONPs

Additionally, the XRD profile revealed a mixed-phase composition, with 30.9% crystalline and 69.1% amorphous content, indicating partial ordering within the BBR-FeONPs matrix. This dual-phase structure may contribute to the unique physicochemical properties of the nanoconjugate.

Scanning Electron Microscopy (SEM) revealed that the BBR-FeONPs possess a predominantly spherical morphology with an irregular and rough surface, likely due to successful berberine conjugation Figure 5. The particles appeared agglomerated, with a size distribution ranging from 21 to 84 nm, and an average particle size of approximately 52 nm.

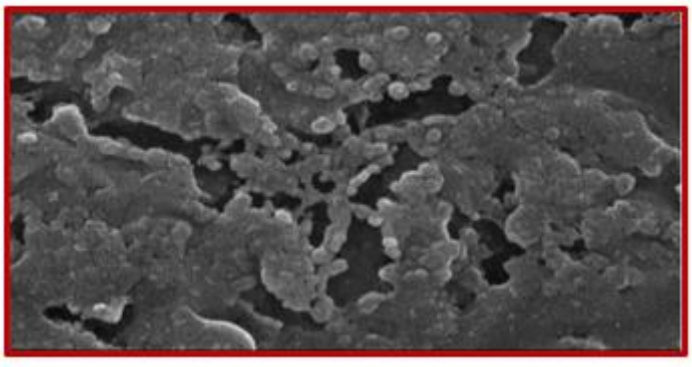

Figure 5. Scanning Electron Microscope of BBR-FeONPs

Transmission Electron Microscopy (TEM) confirmed the nanoscale morphology of BBR-FeONPs, revealing their spherical shape with well-defined boundaries, as shown in Figure 6. These observations support the uniformity and structural stability of the synthesized nanoparticles.

https://doi.org/10.21522/TIJAR.2014.13.03.Art007

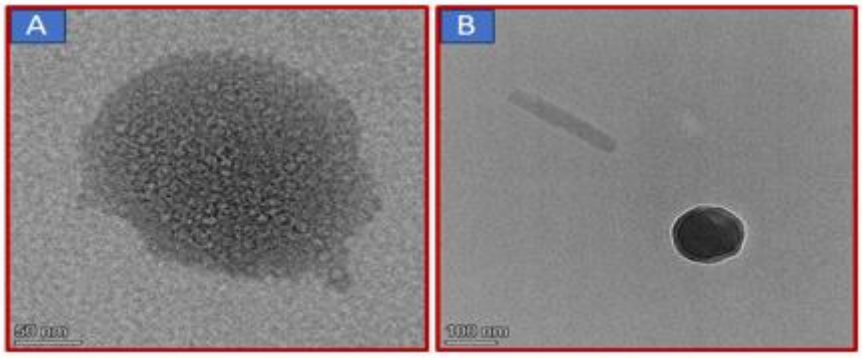

Figure 6. Transmission Electron Microscope of BBR-FeONPs.

Zeta potential analysis was performed to evaluate the surface charge and colloidal stability of BBR-FeONPs. As presented in Table 1, the nanoparticles exhibited a surface charge of -8.3 mV, with a zeta deviation of 4.157 mV, indicating low variability in particle charge. These results, supported by the zeta potential distribution profile shown in Figure 7 and corresponding parameters listed in Table 2, confirm the formation of a moderately stable colloidal dispersion with a uniform charge distribution.

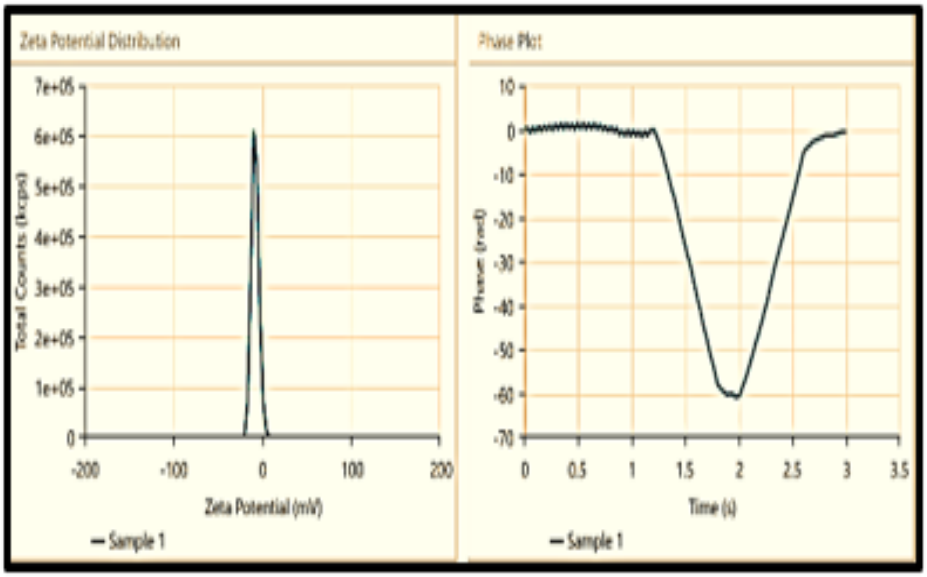

Figure 7. Zeta Potential Measurement of Green Synthesis of BBR-FeONP

Table 1. Specifications for Measuring the Zeta Potential

Zeta potential measurement of BBR-FeONPs	
Zeta Potential (mV)	-8.303
Zeta Peak 1 Mean (mV)	0.1538
Wall Zeta Potential (mV)	-8.709
Zeta Deviation (mV)	4.157
Derived Mean Count Rate (kcps)	1.565E+05
Reference Beam Count Rate (kcps)	2298
Quality Factor	3.437

Table 2. Conditions for Zetapotential Measurements

Conditions for Zeta Potential Measurements	
Dispersant Name	Water
Dispersant RI	1.33
Viscosity (cP)	0.887
Dispersant Dielectric Constant	78.5
Temperature (°C)	25
Cell Description	Zeta DTS1070
Derived Mean Count Rate (kcps)	1.565E+05
Reference Beam Count Rate (kcps)	2298

Quantification of Drug Encapsulation and Loading in BBR-FeONPs

The encapsulation efficiency (EE) and drug loading (DL) of the synthesized BBR-FeONPs were found to be approximately 76% and 7.3%, respectively. These values indicate a high degree of berberine entrapment within the iron oxide nanoparticle matrix.

Antimicrobial Activity of BBR-FeONPs

The current study proved that the antimicrobial activity of BBR-FeONPs was evaluated against *Staphylococcus aureus, Pseudomonas aeruginosa,* and *Escherichia coli* and was determined using the agar well diffusion method, with amoxicillin used as a positive control. The results demonstrated that a clear concentration dose-dependent zone of inhibition was observed across all tested bacterial strains. At the lowest tested concentration (50 µg/mL), BBR-FeONPs showed moderate antimicrobial zones of inhibition of 8 mm, 12.5 mm, and 11 mm against *S. aureus, E. coli*, and *P. aeruginosa,* respectively. Increasing concentration (150 µg/mL) produced zones of inhibition of 13 mm, 15 mm, and 14.3 mm for *S. aureus, E. coli*, and *P. aeruginosa*. Notably, *P. aeruginosa* significantly exhibited the highest zone of inhibition at different concentrations of BBR-FeONPs and showed high antimicrobial activity compared to the other strains. Amoxicillin showed the highest zones of inhibition across all organisms, with diameters of 16.6 mm, 14 mm, and 13 mm for *S. aureus, P. aeruginosa,* and *E. coli* Figure 8.

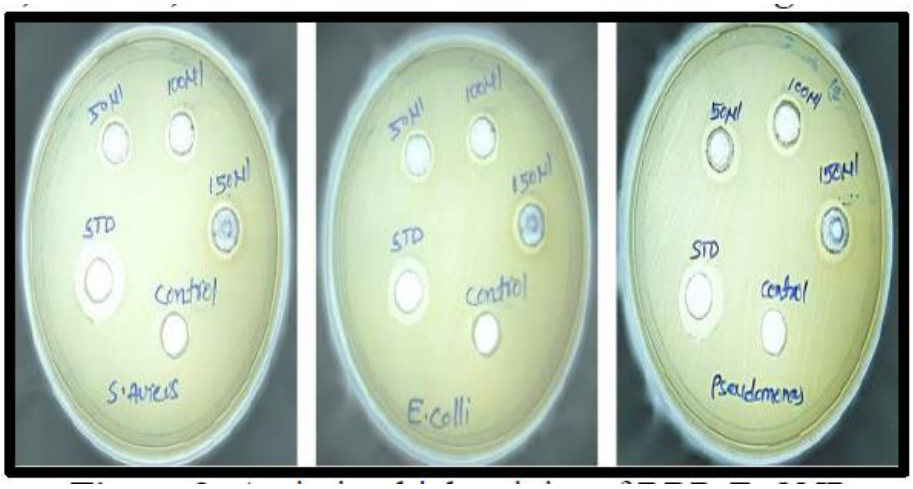

Figure 8. Antimicrobial Activity of BBR-FeONPs

Overall, these findings highlight the promising concentration-dependent antibacterial potential of BBR-FeONPs, particularly against Gram-negative pathogens, and it is statistically significant and p<0.01 Table 3.

Table 3. BBR-FeONPs Comparison of Zone of Inhibition Based on Drug Concentrations and Type of Organisms

BBR-FeONPs Drug Concentrations	S. aureus		P. aeruginosa		E. coli		p-value
	Mean	S.D	Mean	S.D	Mean	S.D	
Amoxicillin	16.6667	0.57735	14	1	13	1	0.005*
50 µg/mL	8	1	12.5	1	11	1	0.01*
100µg/mL	12	1	13	0.70711	12	1	0.2
150 µg/mL	13	1	15	1	14.3333	1.52753	0.19
p-value	0.01*		0.01*		0.01*		

*One Way ANOVA test; *p-value<0.05- statistically significant*

Evaluation of the Cytotoxic Effects of BBR-FeONPs on H460 Non-Small Cell Lung Cancer and HEK293 Human Embryonic Kidney Cells

The cytotoxic potential of synthesized FeONPs, BBR, BBR-FeONPs, and cisplatin was evaluated using the MTT assay on H460 (NSCLC) and HEK-293 cell lines. In H460 cells, FeONPs exhibited a concentration-dependent cytotoxic effect, ranging from 5.16% at 25 µg/mL to 61.29% at 200 µg/mL. BBR, from 9.68% at 25 µg/mL to 74.19% at 200 µg/mL. Notably, the combination of BBR-FeONPs showed enhanced cytotoxicity from 14.19% at 25 µg/mL to 90.97% at 200 µg/mL. Cisplatin, used as a positive control, exhibited 16.16% at 25 µg/mL to 68.39% at 200 µg/mL. All tested compounds demonstrated a clear dose-dependent inhibition, as shown in Figure 9. The mean and SD values of IC50 have been given in Table 4, along with the 95% Confidence Interval. There was a significant difference was observed in IC50 values among all groups (p-value 0.01). However, BBR-FeONPS had a significantly lower IC_{50} value than all other drugs, as shown in Figure 10.

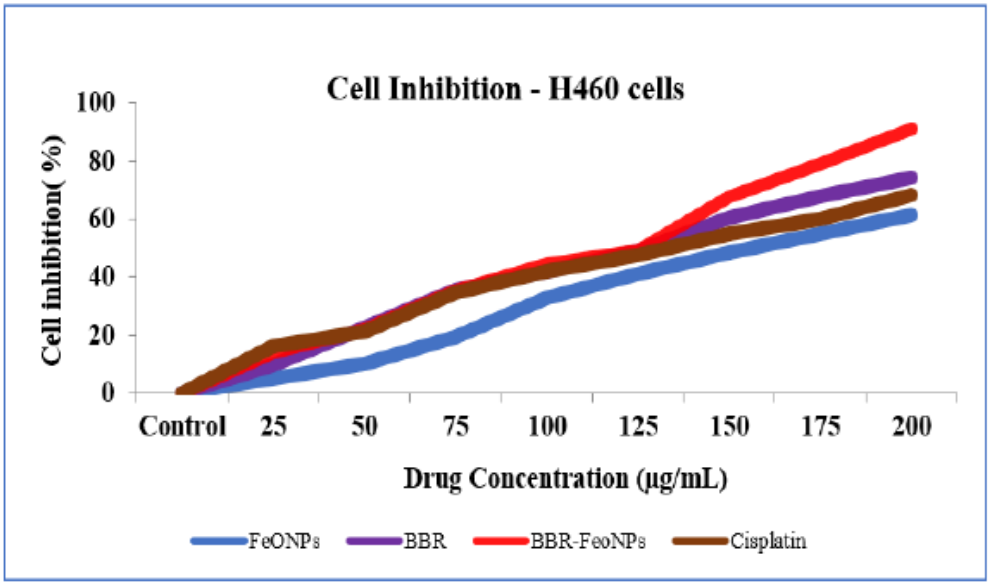

Figure 9. Comparison of Cell Inhibition of FeONPs, BBR, BBR-FeONPs, and Cisplatin on H460 Cells based on Different Concentrations (p-value<0.001; One Way ANOVA test)

https://doi.org/10.21522/TIJAR.2014.13.03.Art007

Table 4. Comparison of IC_{50} Values

	IC_{50}value Mean+SD	**95% Confidence Interval**	**p-value**
FeONPS	58.5+2.1	52.71-61.2	**0.01***
BBR	41.98+4.0	37.65-45.75	
BBR-FeONPS	34.27+2.0	31.50-36.41	
Cisplatin	36.44+3.22	35.20-37.50	

*One Way ANOVA test; *p-value<0.05- statistically significant*

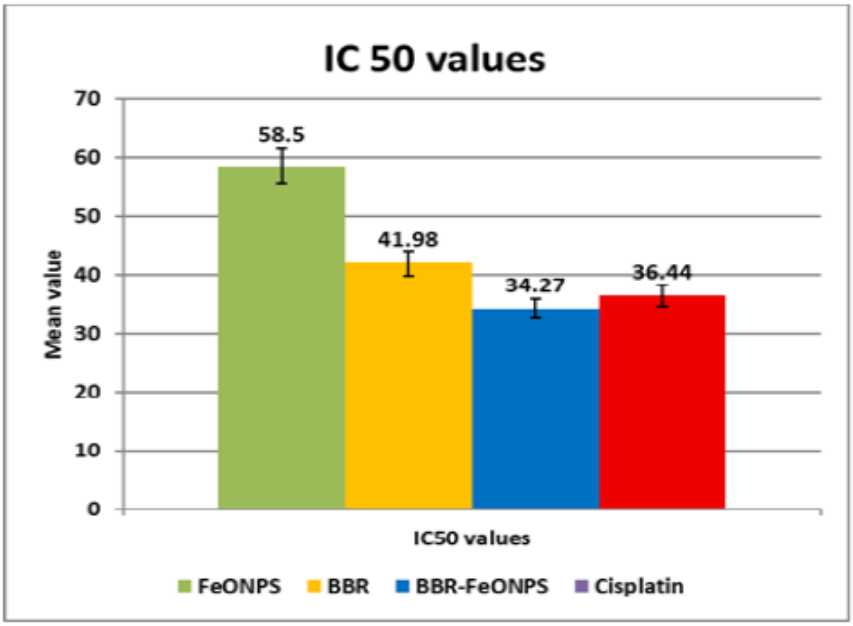

Figure 10. IC_{50} Values of FeONPs, BBR, BBR-FeONPs, and Cisplatin Against H460 Cells

In HEK-293 cells, FeONPs, BBR, and BBR-FeONPs exhibited minimal cytotoxicity, whereas cisplatin demonstrated the highest cytotoxicity at a concentration of 200 µg/mL in 68.39% cell inhibition, as shown in Figure 11.

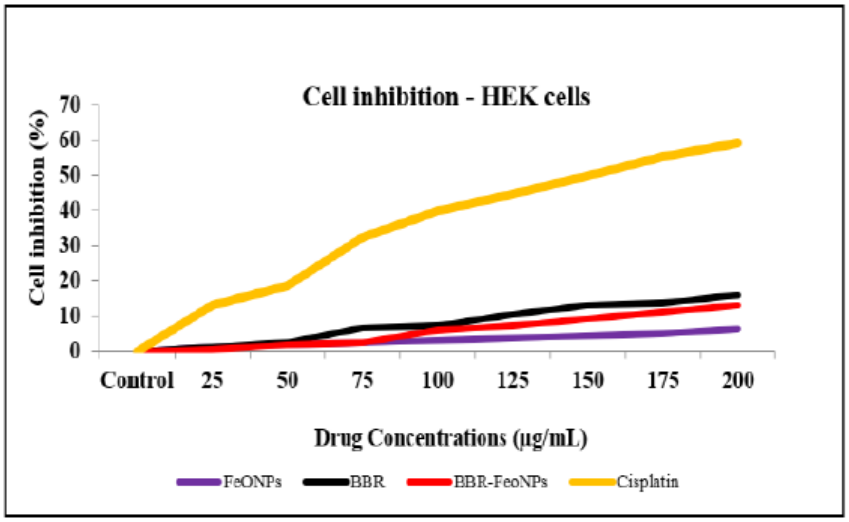

Figure 11. Comparison of Cell Inhibition of FeONPs, BBR, BBR-FeONPs, and Cisplatin on HEK Cells based on Different Concentrations

https://doi.org/10.21522/TIJAR.2014.13.03.Art007

Wound Healing Assay of BBR-FeONPs used in H460 Cells

The anti-migratory effect of BBR-FeONPs on H460 NSCLC cells was assessed using a scratch wound-healing assay, as illustrated in Figure 12.

Our results explained that in the control group, cells exhibited the highest percentage of wound closure, indicating natural cell migration. In contrast, treatment with BBR-FeONPs resulted in significant, concentration-dependent inhibition of cell migration. At a lower concentration of 10 µg/mL, BBR-FeONPs reduced wound closure to 15.99%, indicating a mild inhibitory effect. As the concentration increased, a marked reduction in cell migration was observed: 9.92% at 50 µg/mL, 9.32% at 100 µg/mL, and 6.14% at 200 µg/mL, reflecting a clear dose-dependent inhibition of wound healing. Cisplatin at 200 µg/mL exhibited 9.51% wound closure, which was comparable to the effect of BBR-FeONPs at 100 µg/mL, but significantly less effective than BBR-FeONPs at 200 µg/mL.

Statistical analysis confirmed that the mean wound closure percentage for 200 µg/mL BBR-FeONPs was significantly lower ($p < 0.05$) than that of all other treatment groups, including cisplatin, indicating a superior anti-migratory effect. No statistically significant difference was observed between BBR-FeONPs (100 µg/mL) and cisplatin (200 µg/mL), suggesting a comparable anti-migratory potential at these concentrations Table 5.

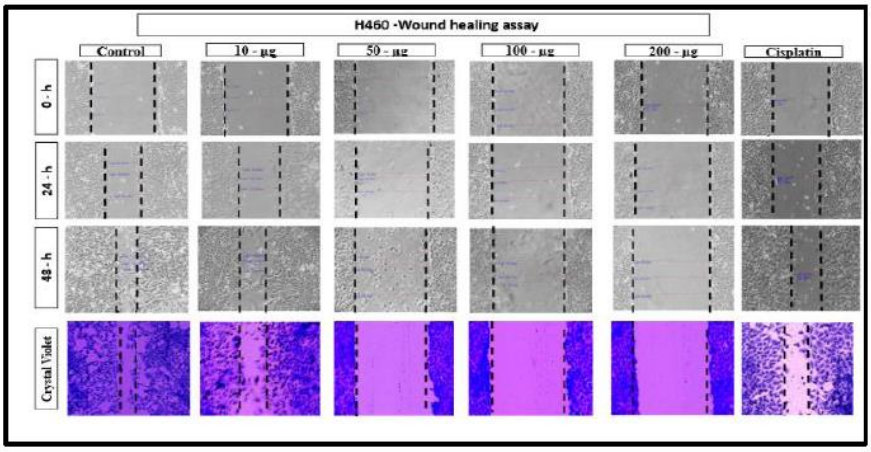

Figure 12. Wound Healing Assay of H460 Cells Treated with BBR-FeONPs and Cisplatin

Table 5. Migration Distance (Mean ± SD) of H460 Cancer Cells Treated with BBR-FeONPs and Cisplatin at Three Time Points

Migration Distance (M+S.D)				
Concentrations	**0 h (T_1)**	**24 h (T_2)**	**48 h (T_3)**	**p-value[a] (0 hr vs 48 hour)**
Control	2230.67+0.0	1574.67+35.6	1086.33+23.45	0.001*
25 µg/mL	2230.67+0.0	1678.67+52.3	1318.33+34.2	0.01*
50µg/mL	2230.67+0.0	1789.67+56.7	1465.67+43.2	0.01*
100µg/mL	2230.67+0.0	2012.32+32.1	1989.23+75.2	0.32
200µg/mL	2230.67+0.0	2121.67+27.8	2012.68+67.8	0.31
Cisplatin	2230.67+0.0	1798.58+34.5	1415.23+56.0	0.01*
p-value[b]	1	0.01*	0.01*	

[a]Paired t-test; *p-value<0.05 –statistically significant; [b]One Way ANOVA test; *p-value<0.05 –statistically significant

Discussion

Iron oxide nanoparticles (FeONPs) were successfully synthesized using the aqueous extract of *Phyllanthus amarus*, which acts as both a natural reducing and stabilizing agent. The synthesized BBR-FeONPs were visually confirmed by the colour change from yellow to dark brown, indicating the successful formation of nanoparticles. The presence of bioactive phytochemicals in the extract, such as phenolics, flavonoids, and carotenoids, played a crucial role in reducing metal ions and acting as a capping agent on the nanoparticles, thereby enhancing their stability. Similar findings have been shown in earlier studies [13, 20].

The use of a green synthesized iron oxide nanoparticle approach is an environmentally friendly, biocompatible, improves drug efficacy and reduces systemic toxicity in cancer therapy. Iron oxide nanoparticles act as magnetic carriers, improving the targeted delivery of berberine to tumour sites, thereby increasing intracellular drug concentration. This targeted delivery not only enhances the therapeutic efficacy of berberine but also minimizes damage to surrounding healthy tissues, making it a promising strategy for cancer treatment [22-24].

The characterization techniques, like UV-Visible Spectroscopy, FTIR, XRD, SEM, TEM, and zeta potential, further validate the formation of BBR-FeONPs. The UV-Visible Spectroscopy observed a peak around 335-342 nm, indicating the successful formulation of berberine-conjugated iron oxide nanoparticles. Similarly, previous studies have reported that Berberine nanoparticles (BBR NPs) exhibited a peak at 344nm [25-27]. FTIR analysis further confirmed the structural integrity and functional group interactions within the synthesized BBR-FeONPs. Characteristic absorption bands corresponding to functional groups such as O–H, C–H, C=C, and Fe-O were observed at approximately 3422, 2366, 1648, 1096, and 625–600 cm^{-1}, respectively. These findings are reported in previous studies [26]. The identified functional groups confirm the successful capping and stabilization of iron oxide nanoparticles by phytochemicals in *P. amarus*, indicating their dual role in reducing metal ions and stabilizing the nanoparticles. This supports the efficiency and confirmation of the synthesis of nanoparticles. The crystalline nature of the synthesized BBR-FeONPs was confirmed by XRD analysis. Characteristic diffraction peaks at 2θ values around 30°, 35°, 43°, 57°, and 63° were observed, closely matching the standard patterns of Fe_3O_4 nanoparticles, thereby validating the successful formation of crystalline iron oxide structures [28].

Morphological analysis using SEM and TEM revealed that the synthesized BBR-FeONPs exhibited a predominantly spherical morphology with an irregular and rough surface, likely due to the surface conjugation of berberine. The average particle size was approximately 52 nm, and slight agglomeration was observed. These findings are consistent with previous reports, where FeONPs synthesized through green methods showed particle sizes ranging from 19 to 40 nm and similar spherical morphology [29]. Earlier studies demonstrated that FeONPs coated with chitosan via both chemical and biological synthesis methods exhibited spherical morphology with an average size of 42.8 nm [30].

Zeta potential analysis indicated that the BBR-FeONPs carried a surface charge of -8.3 mV, suggesting moderate colloidal stability of the nanoparticle suspension. The negative surface charge is likely due to the presence of bioactive phytochemicals acting as capping agents during green synthesis. These findings are consistent with previous studies, including biogenically synthesized FeONPs from *Leptolyngbya* sp., which exhibited a similar zeta potential of -8.5 mV [21]. Similar studies reported zeta potential values of about -19.5 mV, indicating the stable nanoparticle suspensions under physiological conditions

[31]. The observed negative charge contributes to electrostatic repulsion between particles, minimizing aggregation and enhancing dispersion stability.

The anti-microbial activity of BBR-FeONPs was exhibited, dose-dependent, zone of inhibition, against *Pseudomonas aeruginosa, Escherichia coli*, and Staphylococcus aureus. Among them, *P. aeruginosa* has demonstrated the highest sensitivity. This outcome aligns with the initial hypothesis that BBR-FeONPs would exhibit enhanced antimicrobial activity, particularly against Gram-negative bacteria. Compared to the standard drug, BBR-FeONPs showed significant antimicrobial potential, particularly at higher concentrations. This suggests a promising therapeutic role of BBR-FeONPs as alternatives to antibiotics, especially in the antimicrobial resistance.

The observed antibacterial effect is likely attributed to the synergistic action of berberine and iron oxide nanoparticles has reported to disrupt bacterial membranes, induce cytoplasmic leakage, and promote the generation of reactive oxygen species (ROS), leading to oxidative stress and irreversible damage to vital cellular components such as DNA, proteins, and lipids [32, 33]. These mechanisms culminate in bacterial cell death, providing a plausible explanation for the strong bactericidal activity observed in this study. Previous research has shown that the antimicrobial efficacy of berberine-based nanoparticles has concentration-dependent inhibitory zones against *Methicillin-resistant Staphylococcus aureus* (MRSA) and *Escherichia coli* [27]. Overall, BBR-FeONPs showed strong potent antimicrobial activity against multidrug-resistant pathogens.

The cytotoxicity assessment using the MTT assay demonstrated that BBR-FeONPs exhibited significantly enhanced anticancer activity against H460 non-small cell lung cancer (NSCLC) cells compared to FeONPs, BBR alone, and compared to the standard chemotherapeutic agent cisplatin. All tested compounds showed dose-dependent cytotoxicity; however, BBR-FeONPs induced the highest reduction in cell viability, 90.97% at 200 µg/mL, which was statistically significant ($p < 0.01$). In contrast, FeONPs, BBR, and cisplatin exhibited comparatively lower cytotoxic effects against H460 cells, highlighting the superior efficacy of the nano-formulated BBR-FeONPs. Notably, in HEK-293 normal human kidney cells, BBR-FeONPs demonstrated minimal cytotoxicity, whereas cisplatin showed the highest toxic effect at elevated concentrations. These observations are consistent with previous reports, where berberine dose-dependent cytotoxicity in A549 ($IC_{50} = 58.33 \pm 4.96$ µM) and SKOV-3 cancer cells, while showing negligible toxicity in HEK-293 cells [34, 37]. Similarly, FeONPs showed an IC_{50} of 69 ± 0.50 µg/mL in A549 cells [35], and berberine-loaded nanoparticles (BBR-MNPs) exhibited notable cytotoxicity in MDA-MB-231 cells [36]. Furthermore, cisplatin cytotoxicity in HEK-293 cells has been attributed to oxidative stress-mediated mitochondrial damage [38]. Overall, the present findings and existing literature suggest that BBR-FeONPs represent a promising, safer, and more effective alternative to conventional chemotherapy in lung cancer treatment.

The enhanced cytotoxic potential of BBR-FeONPs can be attributed to the synergistic mechanisms contributed by both berberine and iron oxide nanoparticles, which target multiple cellular pathways involved in cancer progression. This enhanced cytotoxicity suggests a synergistic interaction between berberine and FeONPs, likely resulting from multiple complementary mechanisms such as berberine-induced apoptosis via mitochondrial membrane depolarization, activation of caspase-3, modulation of pro- and anti-apoptotic genes (↑Bax, ↓Bcl-2), and inhibition of key survival pathways (PI3K/Akt and MAPK/ERK) [15, 16, 34, 35]. FeONPs contribute to cytotoxicity by generating reactive oxygen species (ROS), which cause

oxidative stress, lipid peroxidation, mitochondrial dysfunction, and DNA fragmentation in cancer cells. By combining these actions, it is intensified to impair cellular repair mechanisms more effectively than either agent alone, confirming the potent synergistic cytotoxic effect of the BBR-FeONP nanocomplex [13, 35].

The wound healing assay results demonstrated that BBR-FeONPs effectively inhibited cell migration in a dose-dependent manner, supressing the anti-migratory efficacy of cisplatin at higher concentrations in H460 cells. The significant reduction in wound closure at 200 µg/mL (6.14%) compared to cisplatin (9.51%) highlights the superior ability of BBR-FeONPs to suppress cellular motility. This enhanced inhibition may be attributed to the synergistic interaction of berberine and FeONPs in disrupting migration-related signalling pathways. Moreover, previous studies have shown that berberine inhibits cell migration in A549, H460, and H1299 NSCLC cell lines in a dose-dependent manner, confirming its inhibitory effect on lung cancer progression [34]. Additionally, berberine significantly inhibited wound closure in HT-29 cells, suggesting that it suppresses the cancer cell migration and metastasis [39].

Conclusion

The green synthesized berberine-loaded iron oxide nanoparticles (BBR-FeONPs) using *Phyllanthus amarus* demonstrated excellent physicochemical stability, potent antimicrobial activity, and anticancer efficacy against H460 NSCLC cells. Furthermore, normal cells (HEK-293) showed low toxicity compared to cisplatin. The anti-migratory effect of BBR-FeONPs was observed as a minimal wound closure compared to the control groups and cisplatin. Overall, these findings highlight that the formulated BBR-FeONPs act as a promising, biocompatible nanoplatform for targeted lung cancer therapy in NSCLC. Further in vivo and mechanistic studies are warranted to validate their clinical applicability.

Author Contributions

M.S. and D.N contributed to conceptualization, methodology, review, and editing. M.S., M.B., performed the experiments and collected the data. M.S., and T.H.H drafted the manuscript G.A.

and D.N. supervised the study and provided technical guidance. M.S. and M.B. performed the statistical analysis. All authors interpreted the results and critically reviewed and revised the final manuscript.

Acknowledgments

Nil.

Conflict of Interest

Nil.

Funding

This research did not receive any specific grant from funding agencies in the public, commercial, or not-for-profit sectors. The study was self-funded by the authors.

Ethical Approval

All experimental procedures involving cell lines were conducted in accordance with institutional research guidelines. As the study involved only established cell lines and did not include human participants or animals, formal ethical committee approval was not required.

Data Availability

The datasets generated and/or analysed during the current study are available from the corresponding author on reasonable request.

Reference

[1]. Bray F, Laversanne M, Sung H, Ferlay J, Siegel RL, Soerjomataram I, et al. Global cancer statistics 2022: GLOBOCAN estimates of incidence and mortality worldwide for 36 cancers in 185 countries. CA Cancer J Clin. 2024;74(3):229-63. https://doi.org/10.3322/caac.21709

[2]. Sathishkumar K, Chaturvedi M, Das P, Stephen S, Mathur P. Cancer incidence estimates for 2022 and projection for 2025: Result from National Cancer Registry Programme, India. Indian J Med Res. 2022;156(4):598-607.

[3]. Nath A, Sathishkumar K, Das P, Sudarshan K, Mathur P. A clinic epidemiological profile of lung cancers in India: Results from the National Cancer Registry Programme. Indian J Med Res. 2022;155(2):264-72.

[4]. Malhotra RK, Manoharan N, Nair O, Deo S, Rath GK. Trends in lung cancer incidence in Delhi, India 1988-2012: Age-period-cohort and joinpoint analyses. Asian Pac J Cancer Prev. 2018;19(6):1647-54.

[5]. Dela Cruz CS, Tanoue LT, Matthay RA. Lung cancer: Epidemiology, etiology, and prevention. Clin Chest Med. 2011;32:605-44. https://doi.org/10.1016/j.ccm.2011.09.001

[6]. Shankar A, Dubey A, Saini D, Singh M, Prasad CP, Roy S, et al. Environmental and occupational determinants of lung cancer. Transl Lung Cancer Res. 2019;8(Suppl 1):S31-49. https://doi.org/10.21037/tlcr.2019.03.11

[7]. Wangmu T, Li C, Han G, Yi P. Berberine restrained proliferation, invasion, and migration by targeting the glycogen synthase kinase 3β/β-catenin pathway in lung adenocarcinoma cells. Oncol Transl Med. 2025. [In press].

[8]. Patra JK, Das G, Fraceto LF, Campos EVR, Rodriguez-Torres MDP, Acosta-Torres LS, et al. Nano based drug delivery systems: Recent developments and future prospects. J Nanobiotechnol. 2018;16:71. https://doi.org/10.1186/s12951-018-0392-8

[9]. Su Z, Dong S, Zhao SC, Liu K, Tan Y, Jiang X, et al. Novel nanomedicines to overcome cancer multidrug resistance. Drug Resist Updat. 2021;58:100777. https://doi.org/10.1016/j.drup.2021.100777

[10]. Madani M, Hosny S, Alshangiti DM, Nady N, Alkhursani SA, Alkhaldi H, et al. Green synthesis of nanoparticles for varied applications: Green renewable resources and energy-efficient synthetic routes. Nanotechnol Rev. 2022;11(1):731-59. https://doi.org/10.1515/ntrev-2022-0063

[11]. Patel JR, Tripathi P, Sharma V, Chauhan NS, Dixit VK. Phyllanthus amarus: Ethnomedicinal uses, phytochemistry and pharmacology: A review. J Ethnopharmacol. 2011;138:286-313. https://doi.org/10.1016/j.jep.2011.09.040

[12]. Thatyana M, Dube NP, Kemboi D, Manicum ALE, Mokgalaka-Fleischmann NS, Tembu JV. Advances in phytonanotechnology: A plant-mediated green synthesis of metal nanoparticles using *Phyllanthus* plant extracts and their antimicrobial and anticancer applications. Nanomaterials. 2023;13(1):176. https://doi.org/10.3390/nano13010176

[13]. Samuel MS, Ravikumar M, John A, Selvarajan E, Patel H, Chander PS, et al. A review on green synthesis of nanoparticles and their diverse biomedical and environmental applications. Catalysts. 2022;12(7):718. https://doi.org/10.3390/catal12070718

[14]. Iqbal MJ, Quispe C, Javed Z, Sadia H, Qadri QR, Raza S, et al. Nanotechnology-based strategies for berberine delivery system in cancer treatment: Pulling strings to keep berberine in power. Front Mol Biosci. 2021;7:624494. https://doi.org/10.3389/fmolb.2020.624494

[15]. Kumar A, Ekavali, Chopra K, Mukherjee M, Pottabathini R, Dhull DK. Current knowledge and pharmacological profile of berberine: An update. Eur J Pharmacol. 2015;761:288-97. https://doi.org/10.1016/j.ejphar.2015.05.068

[16]. Mehra M, Sheorain J, Bakshi J, Thakur R, Grewal S, Dhingra D, et al. Synthesis and evaluation of berberine loaded chitosan nanocarrier for enhanced in-vitro antioxidant and anti-inflammatory potential. Carbohydr Polym Technol Appl. 2024;7:100326.

[17]. Dasari S, Tchounwou PB. Cisplatin in cancer therapy: Molecular mechanisms of action. Eur J

Pharmacol. 2014;740:364-78. https://doi.org/10.1016/j.ejphar.2014.07.025

[18]. Devarajan N, Manjunathan R, Ganesan SK. Tumor hypoxia: The major culprit behind cisplatin resistance in cancer patients. Crit Rev Oncol Hematol. 2021;162:103327. https://doi.org/10.1016/j.critrevonc.2021.103327

[19]. Tarawneh N, Hamadneh L, Abu-Irmaileh B, Shraideh Z, Bustanji Y, Abdalla S, et al. Berberine inhibited growth and migration of human colon cancer cell lines by increasing phosphatase and tensin and inhibiting aquaporins 1, 3 and 5 expressions. Molecules. 2023;28(9):3823. https://doi.org/10.3390/molecules28093823

[20]. Ravi L, Jain P, Maddali V, Madhushree SH, Kajagar S, Doodi S, et al. Green synthesized heteromorphic iron oxide nanoparticles (Fe_3O_4NPs) as potential food additive, food supplement and food colorant sensor and their physiological impact on *Drosophila melanogaster*. Discov Appl Sci. 2025;7(4):225. https://doi.org/10.1007/s42452-025-06592-3

[21]. Minhas LA, Kaleem M, Minhas MAH, Waqar R, Al Farraj DA, Alsaigh MA, et al. Biogenic fabrication of iron oxide nanoparticles from *Leptolyngbya* sp. L-2 and multiple in vitro pharmacogenetic properties. Toxics. 2023;11(7).

[22]. Soetaert F, Korangath P, Serantes D, Fiering S, Ivkov R. Cancer therapy with iron oxide nanoparticles: Agents of thermal and immune therapies. Adv Drug Deliv Rev. 2020;163-164:65-83. https://doi.org/10.1016/j.addr.2020.05.010

[23]. Shestovskaya MV, Luss AL, Bezborodova OA, Makarov VV, Keskinov AA. Iron oxide nanoparticles in cancer treatment: Cell responses and the potency to improve radiosensitivity. Pharmaceutics. 2023;15(4). https://doi.org/10.3390/pharmaceutics15041021

[24]. Kheir MM, Wang Y, Hua L, Hu J, Li L, Lei F, et al. Acute toxicity of berberine and its correlation with the blood concentration in mice. Food Chem Toxicol. 2010;48(4):1105-10. https://doi.org/10.1016/j.fct.2010.01.023

[25]. Hasan E, Manzar Z, Haroon N, Raza A, Ali SN, Lateef M, et al. A facile synthesis of iron oxide nanoparticles as a nano-sensor to detect levofloxacin and ciprofloxacin in human blood and evaluation of their biological activities. RSC Adv. 2024;14(48):36093-100.

[26]. Aisida SO, Madubuonu N, Alnasir MH, Ahmad I, Botha S, Maaza M, et al. Biogenic synthesis of iron oxide nanorods using *Moringa oleifera* leaf extract for antibacterial applications. Appl Nanosci. 2020;10(1):305-15.

[27]. Nguyen HT, Pham TN, Le AT, Thuy NT, Huy TQ, Nguyen TTT. Antibacterial activity of a berberine nanoformulation. Beilstein J Nanotechnol. 2022;13:641-52. https://doi.org/10.3762/bjnano.13.57

[28]. Liu X, Wang J, Chen B, Niu B, Li J. Preparation of berberine magnetic nanoparticles and their inhibition of human gastric cancer BGC-823 cells. AIP Adv. 2024;14(1). https://doi.org/10.1063/5.0123456

[29]. Manzoor N, Ahmed T, Noman M, Shahid M, Nazir MM, Ali L, et al. Iron oxide nanoparticles ameliorated the cadmium and salinity stresses in wheat plants, facilitating photosynthetic pigments and restricting cadmium uptake. Sci Total Environ. 2021;769. https://doi.org/10.1016/j.scitotenv.2020.144466

[30]. Rasheed R, Meera V. Synthesis of iron oxide nanoparticles coated sand by biological method and chemical method. Procedia Technol. 2016;24:210-16. https://doi.org/10.1016/j.protcy.2016.05.030

[31]. Singh K, Chopra DS, Singh D, Singh N. Optimization and ecofriendly synthesis of iron oxide nanoparticles as potential antioxidant. Arab J Chem. 2020;13(12):9034-46. https://doi.org/10.1016/j.arabjc.2020.07.002

[32]. Osman AI, Zhang Y, Farghali M, Rashwan AK, Eltaweil AS, Abd El-Monaem EM, et al. Synthesis of green nanoparticles for energy, biomedical, environmental, agricultural, and food applications: A review. Environ Chem Lett. 2024;22:841-87.

[33]. Antunes Filho S, dos Santos MS, dos Santos OAL, Backx BP, Soran ML, Opriş O, et al. Biosynthesis of nanoparticles using plant extracts and essential oils. Molecules. 2023;28(1):1234.

[34]. Chen QQ, Shi JM, Ding Z, Xia Q, Zheng TS, Ren YB, et al. Berberine induces apoptosis in non-

small-cell lung cancer cells by upregulating miR-19a targeting tissue factor. Cancer Manag Res. 2019;11:9005-15.

[35]. Bharathi D, Preethi S, Abarna K, Nithyasri M, Kishore P, Deepika K. Bio-inspired synthesis of flower-shaped iron oxide nanoparticles (FeONPs) using phytochemicals of *Solanum lycopersicum* leaf extract for biomedical applications. Biocatal Agric Biotechnol. 2020;27:101689. https://doi.org/10.1016/j.bcab.2020.101689

[36]. Madhulatha AVS, Darwin CR. Berberine loaded magnetic nanoparticles for breast cancer therapy on MDA-MB-231 cell lines. Asian J Chem. 2022;34(8):2147-54. https://doi.org/10.14233/ajchem.2022.23784

[37]. Aleissa MS, Al-Zharani M, Alneghery LM, Aleissa AM. Berberine enhances the sensitivity of radiotherapy in ovarian cancer cell line (SKOV-3). Saudi Pharm J. 2023;31(1):110-18. https://doi.org/10.1016/j.jsps.2022.11.006

[38]. Waly MI, Al Moundhri MS, Ali BH. Effect of curcumin on cisplatin- and oxaliplatin-induced oxidative stress in human embryonic kidney (HEK) 293 cells. Ren Fail. 2011;33(5):518-23.

[39]. Huang C, Liu H, Yang Y, He Y, Shen W. Berberine suppressed the epithelial-mesenchymal transition (EMT) of colon epithelial cells through the TGF-β1/Smad and NF-κB pathways associated with miRNA-1269a. Heliyon. 2024;10(16):e28194. https://doi.org/10.1016/j.heliyon.2024.e28194